

# Spatially weighted BOLD signal for comparison of functional magnetic resonance imaging and near-infrared imaging of the brain

Angelo Sassaroli,<sup>a,\*</sup> Blaise deB. Frederick,<sup>b</sup> Yunjie Tong,<sup>a</sup> Perry F. Renshaw,<sup>b</sup> and Sergio Fantini<sup>a</sup>

<sup>a</sup>Department of Biomedical Engineering, Tufts University, 4 Colby Street, Medford, MA 02155, USA

<sup>b</sup>Brain Imaging Center, McLean Hospital, 115 Mill Street, Belmont, MA 02478, USA

Received 5 May 2006; revised 5 July 2006; accepted 12 July 2006

Available online 30 August 2006

We introduce a weighted spatial average of the functional magnetic resonance imaging (fMRI) BOLD signal (blood oxygen level-dependent) that is appropriate for comparison with the changes in oxy- and deoxy-hemoglobin concentrations measured with near-infrared spectroscopy (NIRS) during brain activation. Because the BOLD signal shows a spatial dependence (both in shape and amplitude) within the region of activation, the location of the optical probe with respect to the region of BOLD activation should be taken into account for comparison of the BOLD and NIRS signals. Our new method is based on combining weighted contributions of the BOLD signal from each activated voxel, with a weight given by a hitting density function for photons migrating between a given pair of illumination and collection points. We present a case study where we have found that the new spatially weighted BOLD signal shows a high spatial and temporal correlation with the oxy- and deoxy-hemoglobin concentration changes measured with NIRS during a hand-tapping protocol. These findings reinforce the idea that fMRI and NIRS are sensitive to similar underlying hemodynamic changes, and indicate that the proposed weighted BOLD signal is needed for a quantitative comparison of BOLD and NIRS signals.

© 2006 Elsevier Inc. All rights reserved.

## Introduction

The importance of NIRS in functional imaging of the brain is due to several unique features such as its ability to non-invasively detect the concentrations of oxy-hemoglobin and deoxy-hemoglobin, its relatively high temporal resolution (down to about 10 ms), the fact that it is relatively insensitive to subject's motion, and its cost-effectiveness. NIRS features a relatively low spatial resolution (5–10 mm), which is nevertheless comparable with the resolution obtained with fMRI during brain studies. In principle, much higher resolutions are possible for fMRI (down to 100  $\mu$ M), however, those require longer acquisition times, restricted fields of view and/or parallel acquisition hardware.

The reason for the low resolution in NIRS is that most biological tissues are highly scattering media in the wavelength range 690–900 nm, and only diffused photons can be detected after undergoing hundreds of isotropic-equivalent scattering events, which obviously degrades the image quality of the probed region. The main drawback of NIRS with respect to fMRI is the limited sensitivity to hemodynamic changes occurring deeper in the tissue. The average penetration depth of detected photons depends on several parameters and in principle can be increased by increasing the source-detector distance at the expense of the signal-to-noise ratio (Del Bianco et al., 2002). Usually, in brain imaging one can detect hemodynamic changes that occur at a maximum depth of 2–3 cm. However, the brain cortex, which plays a major role in the functional activities of the brain, is mostly accessible to near-infrared light. Several NIRS studies have been reported on functional imaging of the human brain during motor (Franceschini et al., 2000; Toronov et al., 2000; Wolf et al., 2002; Boas et al., 2001; Strangman et al., 2003), auditory (Kennan et al., 2002), cognitive (Hoshi and Tamura, 1993; Watanabe et al., 1998) and visual (Wolf et al., 2002; Csibra et al., 2004) activation.

While fMRI offers the advantage of a relatively higher spatial resolution and sensitivity to deeper regions of the brain, it is also particularly sensitive to motion artifacts (therefore, it cannot be performed, for example, on newborn infants in the awake state) and it requires bulky and expensive instrumentation. The best practical temporal resolution of fMRI is on the order of one second. In fact we remind that the temporal resolution of fMRI depends on experimental choices of slice thickness, number of slices, and the scanner's fundamental limit on acquisition time for sequential slices (and to a lesser degree, available signal to noise ratio). For example with the MRI hardware used in this work, we can collect 15 slices per second, and to cover our area of interest, we use thirty 3-mm-thick slices, which takes a minimum of 2 s to acquire. The origin of the fMRI BOLD signal has been the object of extensive theoretical and experimental studies (Ogawa et al., 1993; Boxerman et al., 1995; Buxton and Frank, 1997; Buxton et al., 1998, 2004; Obata et al., 2003; Seiyama et al., 2004). Currently, the most accredited theories (Buxton et al., 1998; Ogawa et al., 1993; Boxerman et al., 1995)

\* Corresponding author.

E-mail address: [angelo.sassaroli@tufts.edu](mailto:angelo.sassaroli@tufts.edu) (A. Sassaroli).

Available online on ScienceDirect ([www.sciencedirect.com](http://www.sciencedirect.com)).

identify the change in deoxy-hemoglobin concentration and blood volume as the major sources of the BOLD signal.

Several works have already been published in the literature about concurrent fMRI-NIRS experiment during motor (Toronov et al., 2003; Strangman et al., 2002, Siegel et al., 2003), and cognitive (Toronov et al., 2001; Chance et al., 1998) activation of the brain. At this level of development of the two independent methodologies, NIRS and BOLD signals are synergistic for a better understanding of the hemodynamic changes involved during brain activation. In the concurrent experiments, fMRI is often considered the “gold standard”, at least for its detailed spatial information. However, the biophysical origin of the BOLD signal is not totally clear and comparison with the changes in oxy- and deoxy-hemoglobin concentrations measured with NIRS has given sometimes conflicting results. Strangman et al. observed a good match between BOLD signal and the change in oxy-hemoglobin concentration (Strangman et al., 2002), whereas Toronov et al. observed a better match between BOLD signal and deoxy-hemoglobin concentration changes (Toronov et al., 2003). Yamamoto and Kato (2002), in a combined fMRI-NIRS experiment, found that both MR signals and deoxy-hemoglobin content increased in Broca's area during a language task. Moreover, the authors found that all of the fMRI changes correlated with changes in oxy-hemoglobin. Toronov et al. have assigned the origin of these discrepancies to the particular experimental method used for the acquisition of the optical data (e.g., single distance versus multi-distance arrangement of the source-detector couples) (Toronov et al., 2003). Other investigators have argued that these discrepancies may be due to the intrinsic sensitivity of BOLD signal to different vascular compartments in presence of stronger or weaker static magnetic field. In the work of Seiyama et al. (2004), the authors used the model proposed by Kim et al. (1999) to derive the change in BOLD signal from functional parameters like the change of oxygen saturation in tissue and the change in total hemoglobin. The model is also based on a specific parameter which is a function of the vessel size. One of the conclusions of the study is that fMRI signals obtained with 1.5 T MRI scanners are sensitive mainly to venules and larger veins (vein model) and that the capillaries play a role only for higher values of the static field ( $>4$  T). Similar arguments were used by Yamamoto and Kato (2002) to explain the discrepancy of NIRS data with the canonical BOLD theory. In particular, the authors pointed out that an extravascular contribution to the fMRI signal becomes more predominant at higher magnetic fields and this effect was not accounted for in the original model of Buxton et al. (1998). In the work of Yamamoto et al., one can find a list of published works where the canonical BOLD theory (which attributes the positive changes in signal mainly to a decrease in deoxy-hemoglobin content) was not supported by NIRS outcomes. Therefore, while the origin of the signal in NIRS is more directly attributed to hemoglobin concentration and saturation, the hemodynamic origin of the BOLD signal is dependent on more variables and this might be the reason of the discrepancy found between the two methodologies in several studies.

Despite the validity of these conceptual reasons that might account for the different information content of NIRS and fMRI data, in this work, we argue that a meaningful comparison of fMRI and NIRS data must take into account the spatial origin of the signals to be compared. Usually, a unique BOLD signal representing the average response to the stimulus is derived from the whole activated region. In this study, we show that the BOLD signal can

show a strong spatial dependence within the activated area, not only in terms of the amplitude of activation but also in terms of the nuances of the temporal shape. Therefore, we argue that using a single BOLD signal may cause a misleading comparison of NIRS and fMRI data. For example, if a particular source-detector pair samples a peripheral region of activation, NIRS is sensitive only to hemodynamic changes occurring in that region, which might be different from those in other regions. We therefore suggest that the correlation of NIRS and BOLD data should be carried out by taking into account the location of the activated area with respect to the position of each optical source-detector pair. To this aim, we propose a new way to calculate the BOLD signal that uses a weight function given by the hitting density of photons migrating between a given light source and optical detector. The weight function is defined by using a semi-infinite homogenous diffusive model. This approximation for the heterogeneous tissue under consideration is justified by two considerations. Firstly, the average optical properties of the medium provide a spatial distribution of the weight function that does not deviate dramatically from the actual one, which is determined by a generally unknown spatial distribution of the optical properties of tissue. Secondly, as we have found in this work, the relatively weak dependence of the weight function geometry on the average optical properties results in a quantitative comparison of the new proposed BOLD signal with NIRS data that is not significantly affected by the choice of the optical properties (and therefore by the inhomogeneity of the tissue). We present one case study where the newly defined BOLD signal is calculated for each source-detector pair, and it shows an excellent agreement with the spatial/temporal properties of the changes in oxy- and deoxy-hemoglobin measured with NIRS during a hand-tapping protocol. These findings suggest that a similar underlying mechanism is at the origin of BOLD and NIRS data, at least for this choice of field strength (3T), and show the important role that the newly defined weighted BOLD signal can play in the quantitative comparison of fMRI and NIRS.

## Methods

The experiment was carried out with a near-infrared tissue imager (Imagent, ISS, Inc., Champaign, IL) comprising sixteen laser sources at 690 nm, sixteen laser sources at 830 nm (average power of about 1 mW) and four optical detectors (photomultiplier tubes, Hamamatsu Photonics R928). The laser diodes were coupled to optical fibers (400  $\mu\text{m}$  in core diameter and 10 m long), that delivered the light to the head of the subject. The optical signals were collected on the head of the subject by means of four optical fiber bundles (3 mm in diameter and 10 m long) that delivered the collected light to the detectors. The sixteen lasers on one side of the brain were sampled at a frequency of 6.25 Hz, so that each laser was on for 10 ms per cycle, and two laser sources (on opposite sides of the brain) were on at the same time. Tests run on various subjects have showed that cross-talk among the channels was negligible. More details on the principle of the experimental apparatus can be found in the work of Fantini and Franceschini (2002). A special fMRI compatible helmet was designed to hold the source and detector fibers and to fit comfortably on the head of the subject. The source-detector distance was fixed at 3.5 cm for each NIRS channel. To improve the coupling of the optical fibers at each location on the head, elastic bands were used in conjunction with a retractable and resilient set of optical fibers to better control

the contact pressure exerted by the fibers on the scalp. The acquisition of fMRI and optical signals was synchronized electronically to generate a common time axis for the BOLD and NIRS data. A schematic diagram of the experimental apparatus and the location of the illumination and collection optical fibers on the subject's head is shown in Fig. 1.

The finger-tapping protocol started with 1 min of baseline acquisition, during which the subject (a healthy 30-year-old male), was lying comfortably on the fMRI bed while staying motionless and relaxed. Following the baseline acquisition, the subject performed a series of six finger tapping/rest periods, first with the right hand and then with the left hand, each made of 20 s of finger tapping followed by 20 s of rest. The finger tapping was done by tapping four fingers against the thumb at a frequency of about 2–3 Hz. The optical data were analyzed by using standard algorithms to filter out unwanted frequencies prior to applying a folding average procedure. More precisely, we used a non-recursive time-domain filter with a band pass of 0.0125–0.4 Hz that is a built-in function in Matlab 7.04 (The Mathworks, Natick, MA). NIRS intensity data were translated into temporal changes in the concentrations of oxy-hemoglobin ( $\Delta[\text{HbO}]$ ) and deoxy-hemoglobin ( $\Delta[\text{Hb}]$ ) according to the differential pathlength factor (DPF) method (Matcher et al., 1993; Sassaroli and Fantini, 2004). For the DPF, we have used published values of 6.51 at 690 nm, and 5.86 at 830 nm. Despite the limitations of the DPF method for absolute quantitation of the changes in oxy-hemoglobin and deoxy-hemoglobin, it has been proven that a proper choice of the wavelength pair (like 690 and 830 nm) significantly decreases the cross-talk between the two species (Strangman et al., 2003; Uludag et al., 2004; Yamashita et al., 2001). As for the spatial mapping of  $\Delta[\text{HbO}]$  and  $\Delta[\text{Hb}]$ , we used a back-projection algorithm (Franceschini et al., 2000).

The fMRI scanner used for the experiments was a Siemens Trio 3 T scanner. The fMRI data processing was done as follows. After localization and shimming, a series of fMRI images are acquired. Image parameters are as follows: gradient echo EPI, TE/TR=30/2020 ms, 64×64 image matrix, full k-space acquisition, FOV 220×220, 30 interleaved coronal slices (R/L readout), 3 mm thick, 0 mm gap, with the slice stack centered on the motor strip. 120 time points are acquired after 12 dummy shots. The update rate of fMRI data was 0.5 Hz. Images are saved in DICOM format and processed using Brain Voyager QX (Brain Innovations B.V., Maastricht, Netherlands) using the following steps: the time

courses were corrected for slice acquisition timing, and 3D motion corrected, spatially filtered in 3D with a 5-mm Gaussian Kernel, and temporally filtered using linear trend removal, high pass filtered at 1/240 Hz, and temporally smoothed with a 2.8-s Gaussian kernel. Data were then re-sampled onto a 3-mm isotropic three-dimensional grid aligned with the anatomic image. For the spatial and temporal correlation of fMRI and NIRS signals, it is critical to know the exact location of the optical fibers on the subjects head. This was done by using the anatomical MRI scan which is sensitive to the small perturbations induced by the fibers on the head surface. Usually it is possible to locate the position of all the fibers even though the marks from one or two fibers might not be particularly visible in the MRI anatomical scan, since all the other visible points constrict the location of the whole helmet.

The method that we are proposing for calculating the spatially weighted BOLD is based on the following photon-hitting density function (Feng et al., 1995):

$$P_n(x,y,z) = \frac{z^2 \exp\{-k\{(x^2 + y^2 + z^2)^{1/2} + [(d-x)^2 + y^2 + z^2]^{1/2}\}\}}{(x^2 + y^2 + z^2)^{3/2} [(d-x)^2 + y^2 + z^2]^{3/2}} \times [k(x^2 + y^2 + z^2)^{1/2} + 1] \{k[(d-x)^2 + y^2 + z^2]^{1/2} + 1\} \quad (1)$$

In Eq. (1)  $P_n(x, y, z)$  is the photon-hitting density function, which is proportional to the probability density per unit volume that a photon injected at  $(0, 0, 0)$  and detected at  $(d, 0, 0)$  crosses the generic point  $(x, y, z)$ . The function  $P_n(x, y, z)$  describes the perturbation induced by a point-like absorbing spherical defect at  $(x, y, z)$  in an otherwise homogenous, semi-infinite medium. The coefficient  $k$  (effective attenuation coefficient) is defined as  $k = (3 \mu_a \mu'_s)^{1/2}$ , where  $\mu_a$  is the absorption coefficient, and  $\mu'_s$  is the reduced scattering coefficient of tissue. For each NIRS source-detector pair, we define a photon migration averaged (PMA) BOLD signal as follows:

$$BOLD_{PMA}(t) = \frac{\int_V BOLD_{raw}(x,y,z,t) P_n(x,y,z) dx dy dz}{\frac{1}{T} \int_0^T dt \int_V BOLD_{raw}(x,y,z,t) P_n(x,y,z) dx dy dz} \quad (2)$$

where  $BOLD_{PMA}(t)$  is the proposed photon migration-averaged BOLD at time  $t$ , and  $BOLD_{raw}(x, y, z, t)$  is the standard BOLD signal at time  $t$  and position  $(x, y, z)$ . The temporal average is carried out for the whole duration of the measurement ( $T$ ). In the last step, we apply a standard folding average procedure to

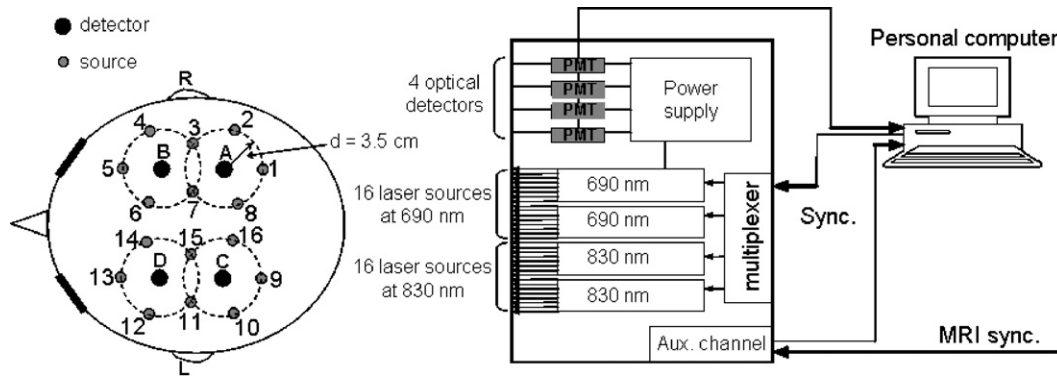


Fig. 1. Schematic diagram of the experimental apparatus. The 32 laser diodes (16 emitting at 690 nm, and 16 at 830 nm) and the 4 photomultiplier tube (PMT) detectors are all coupled to optical fibers. The source fiber locations (each containing one source fiber at 690 nm and one at 830 nm) on the subject's head are numbered from 1 to 16. The four detector fibers are labeled A to D.

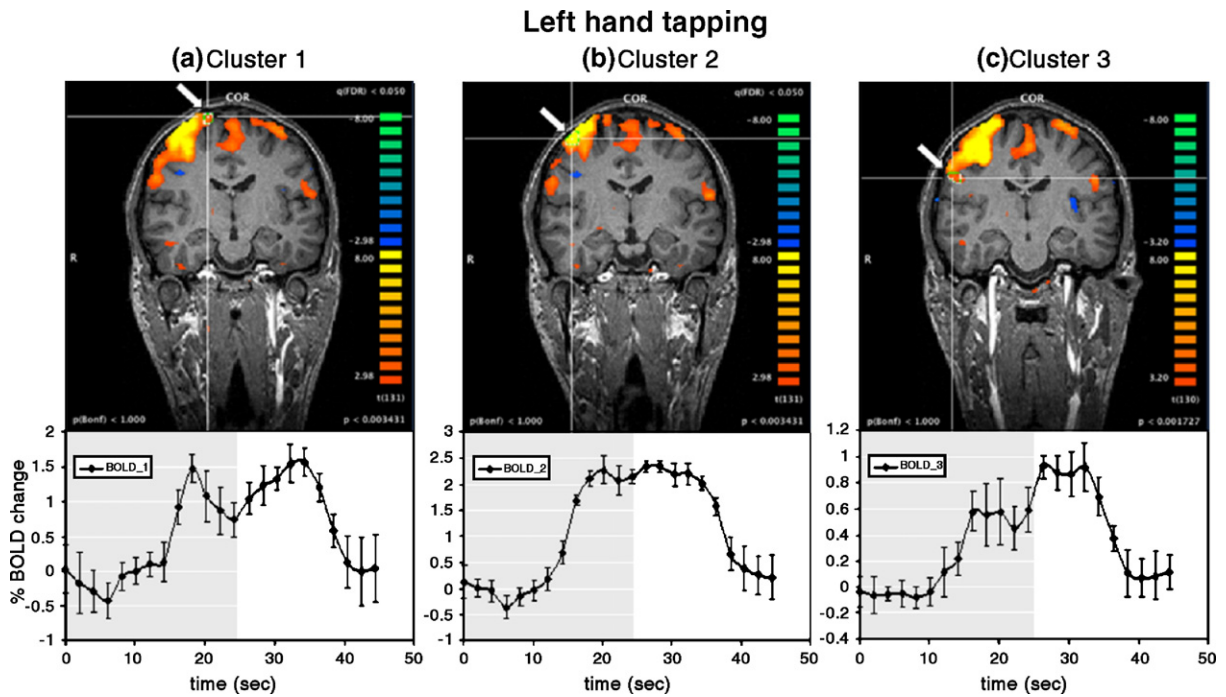


Fig. 2. Standard BOLD signals measured during left hand tapping. The top figures are maps of the distribution of the BOLD signal, while the bottom graphs are the folding average BOLD signals over the tapping/rest period as measured at different clusters of voxels (indicated by the white arrows in the corresponding top panels) within the activated region. Note the different amplitude and temporal shape of the standard BOLD signal at the three different clusters of voxels.

$BOLD_{PMA}(t)$  to obtain the  $BOLD_{PMA}$  response during the activation-rest period.

**Results and discussion**

*Spatial dependence of the BOLD signal*

Fig. 2 shows how the BOLD signal can vary significantly within the region of brain activation (during left finger tapping in

this case). The bottom panels represent the folding average of the standard BOLD signal measured at the locations indicated by the white arrow in the corresponding top panels. We notice that both the intensity of the activation (expressed in percent changes from the baseline value), and the shapes of the temporal trends are different. This result supports our point that a proper spatial weight function should be applied to the BOLD signals before comparison with optical data. To the best of our knowledge, the spatial dependence of BOLD signal has not been discussed in previous works. The spatial dependence of BOLD signal might be caused by different hemodynamic responses around the region of activation,

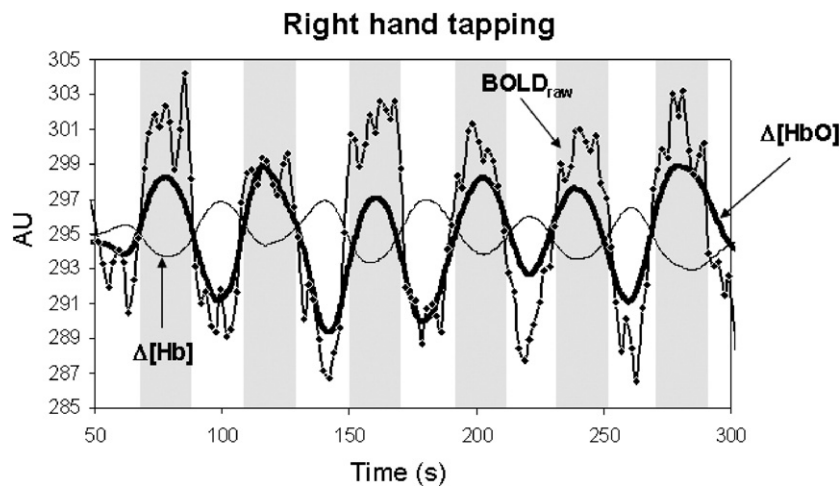


Fig. 3. Temporal traces of the standard BOLD signal ( $BOLD_{raw}$ ),  $\Delta[Hb]$  and  $\Delta[HbO]$  at channel C-11 during six tapping/rest periods (right hand tapping). The tapping periods are indicated by the shaded areas. The traces of  $\Delta[Hb]$  and  $\Delta[HbO]$  have been shifted and normalized for comparison.

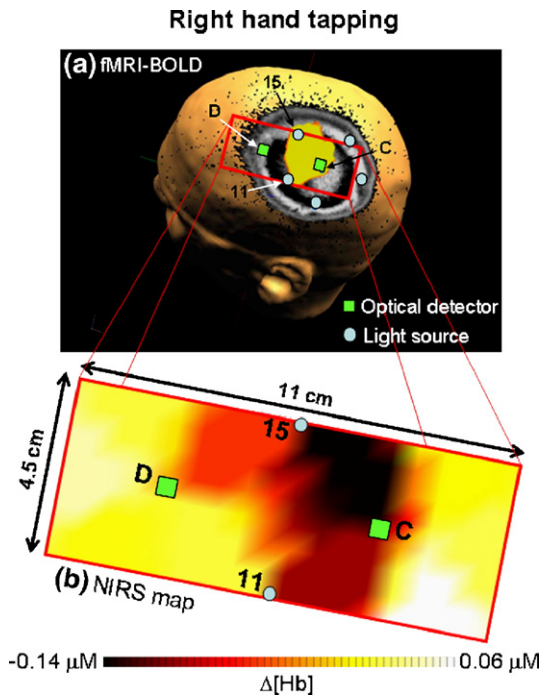


Fig. 4. Comparison of the activated areas obtained during right hand tapping with (a) fMRI BOLD and with (b) NIRS data. The MRI map shows a cross section of the subject’s head, at a depth of 5 mm into the brain, which is parallel to the plane of the NIRS optical fibers. The location of detector C and some of the source fibers used for co-registration of the NIRS map are shown in the MRI image. The NIRS map is measured 9.6 s after the onset of hand tapping.

not only in terms of intensity of activation (reflecting the distance of each voxel from the activated neurons) but also in terms of local temporal features since it is reasonable to think that the hemodynamic change is spreading from a focal point to a larger region.

*NIRS and standard BOLD signals during right finger tapping*

Fig. 3 shows a comparison of the temporal evolution of the standard BOLD signal and the changes of oxy- and deoxy-hemoglobin concentrations during the right finger tapping protocol, including all six tapping/rest periods. The tapping periods are represented by the shaded areas. The changes in [Hb] and [HbO] have been shifted by adding a constant value and multiplied by a factor for comparison with the BOLD signal, and they refer to source-detector pair C-11. This figure shows the opposite behavior of oxy- and deoxy-hemoglobin, with [HbO] increasing and [Hb] decreasing during the tapping task. One can describe this typical opposite behavior of the two hemoglobin species with a  $\pi$  phase shift. However, the literature has also reported phase differences of [Hb] and [HbO] different than  $\pi$ . A possible explanation of this intermediate behavior is found in the work of Fantini (2002).

Fig. 4(a) illustrates the standard BOLD activated area (yellow-shaded area) within a cross section that is parallel to the plane of the NIRS optical fibers, and at a depth of 5 mm into the brain, or  $\approx 15$  mm from the scalp. In particular, detector fiber C and source fibers 11 and 15 are superimposed to the MRI image to show their location on the subjects head for NIRS co-registration. Fig. 4(b) reports the corresponding spatial map of the changes in [Hb] measured with NIRS at 9.6 s after onset of activation. One can see an excellent spatial correlation between the activated motor area of the brain as measured by fMRI and the spatial distribution of  $\Delta[\text{Hb}]$  as measured by NIRS. In fact, both fMRI and NIRS detect an activated cortical area located between detector C and sources 11 and 15 during right finger tapping. The optical maps can be organized in a real-time movie, as previously reported by Franceschini et al. (2000); these can add valuable information on the temporal evolution of the activated area during the task. The darker area in the  $\Delta[\text{Hb}]$  map corresponds to a decrease in cerebral [Hb] with respect to the baseline. Since the change in oxy- and deoxy-hemoglobin expected from functional tasks is typically focal, the use of the DPF method for data analysis is expected to cause an underestimation of the changes (partial volume effect). However, while the absolute changes may be

**Photon-hitting density function for channel C-11, and BOLD activated area**

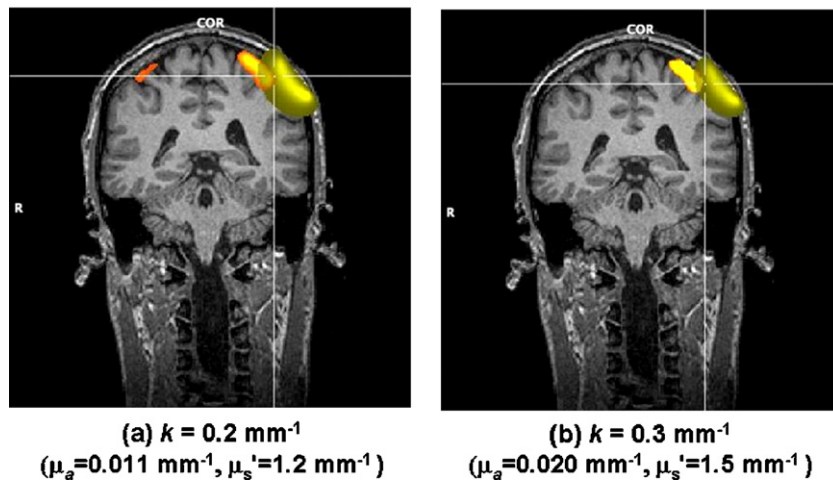


Fig. 5. Representation of the “banana shapes,” or photon-hitting density function (in light yellow) for channel C-11, and its overlap with the activated brain region as measured with fMRI BOLD (dark yellow) during right hand tapping. The calculation of the photon-hitting density function has been performed for (a)  $k=0.2 \text{ mm}^{-1}$ , and (b)  $k=0.3 \text{ mm}^{-1}$ .

underestimated, the direction (increase or decrease), the temporal shape, and the spatial features of the concentration changes are expected to be reliable.

#### NIRS and the new photon migration averaged BOLD signal

In Fig. 5, we show a superposition of the optical “banana shape” (Feng et al., 1995; Schotland et al., 1993), or region of optical sensitivity, for optical channel C-11 (light yellow), and the activated area detected by BOLD-fMRI (dark yellow). The calculation of the banana shape has been carried out for  $k=0.2 \text{ mm}^{-1}$  (panel (a)) and  $k=0.3 \text{ mm}^{-1}$  (panel (b)). Because the optical helmet is not devised for multi-distance measurements (Fantini et al., 1999) of the absolute optical properties, we have considered different values of  $k$  to study the sensitivity of the results on the choice of the effective attenuation coefficient. As shown in Fig. 5(b), a greater value of  $k$  corresponds to a shallower region of optical sensitivity and a reduced overlap with the BOLD region of activation.

Fig. 6 reports a comparison of the temporal traces of  $-\Delta[\text{Hb}]$ ,  $\Delta[\text{HbO}]$  and  $BOLD_{PMA}$  at channels B-3, B-4, B-5, and B-7 (see Fig. 1 for the location of these optical channels) during left hand tapping. The calculation of  $BOLD_{PMA}$  was carried out for a typical value of the effective attenuation coefficient for biological tissues of  $k=0.23 \text{ mm}^{-1}$  (which corresponds, for example, to an absorption coefficient of  $0.015 \text{ mm}^{-1}$  and a reduced scattering coefficient of  $1.2 \text{ mm}^{-1}$ ). To compare the shape of the temporal traces, we have introduced an arbitrary normalization factor, and the trend of  $\Delta[\text{Hb}]$  has been inverted. In Fig. 6, one can observe that for any given channel, the NIRS and  $BOLD_{PMA}$  data have very similar temporal trends, while different channels show different behaviors. For example, the  $BOLD_{PMA}$ ,  $\Delta[\text{HbO}]$  and  $-\Delta[\text{Hb}]$  all peak during left hand-tapping (at  $t \sim 14 \text{ s}$ ) at channel

Table 1

Correlation coefficients between  $BOLD_{PMA}$  and change of  $[\text{Hb}]$  and  $[\text{HbO}]$  during left hand tapping

Channel	$r_{-\Delta[\text{Hb}]\text{-BOLD}}$	$r_{\Delta[\text{HbO}]\text{-BOLD}}$
B-3/B-3	0.78	0.87
B-4/B-4	0.63	0.76
B-5/B-5	0.86	0.87
B-7/B-7	0.91	0.96
B-3/B-4	-0.34	-0.17
B-5/B-4	0.04	0.09
B-7/B-4	-0.35	-0.28

The first column indicates the optical channel (see Fig. 1). In the second and third columns are written the values of the correlation coefficients between  $BOLD_{PMA}$ ,  $\Delta[\text{Hb}]$ , and  $\Delta[\text{HbO}]$  in the same channel (first four rows) and in different channels (last three rows). In the latter case the correlation coefficient was calculated by using the  $BOLD_{PMA}$  of channel B4 with NIRS data of channels B3, B5, B7, respectively.

B-7, while they show an early peak (at  $t \sim 5 \text{ s}$ ) and a delayed post-tapping recovery at channel B-4. A quantitative correlation analysis of the NIRS and  $BOLD_{PMA}$  data in the temporal range of 2–30 s yields the following values for the correlation coefficients:  $r_{-\Delta[\text{Hb}]\text{-BOLD}}=0.78, 0.63, 0.86, 0.91$  and  $r_{\Delta[\text{HbO}]\text{-BOLD}}=0.87, 0.76, 0.87, 0.96$  for channels B-3, B-4, B-5, B-7, respectively. We usually do not get such high correlation coefficients between NIRS and  $BOLD_{PMA}$  data across different channels. For example, if we correlate the NIRS data of channel B-3 with  $BOLD_{PMA}$  of channel B-4 we find  $r_{-\Delta[\text{Hb}]\text{-BOLD}}=-0.34$  and  $r_{\Delta[\text{HbO}]\text{-BOLD}}=-0.17$ . If we correlate the NIRS data of channel B-7 with  $BOLD_{PMA}$  of channel B-4 we find  $r_{-\Delta[\text{Hb}]\text{-BOLD}}=-0.35$  and  $r_{\Delta[\text{HbO}]\text{-BOLD}}=-0.28$ . Finally, if we correlate the NIRS data in channel B-5 with  $BOLD_{PMA}$  of channel B-4, we find  $r_{-\Delta[\text{Hb}]\text{-BOLD}}=0.04$  and  $r_{\Delta[\text{HbO}]\text{-BOLD}}=0.09$ . These results are summarized in Table 1. We

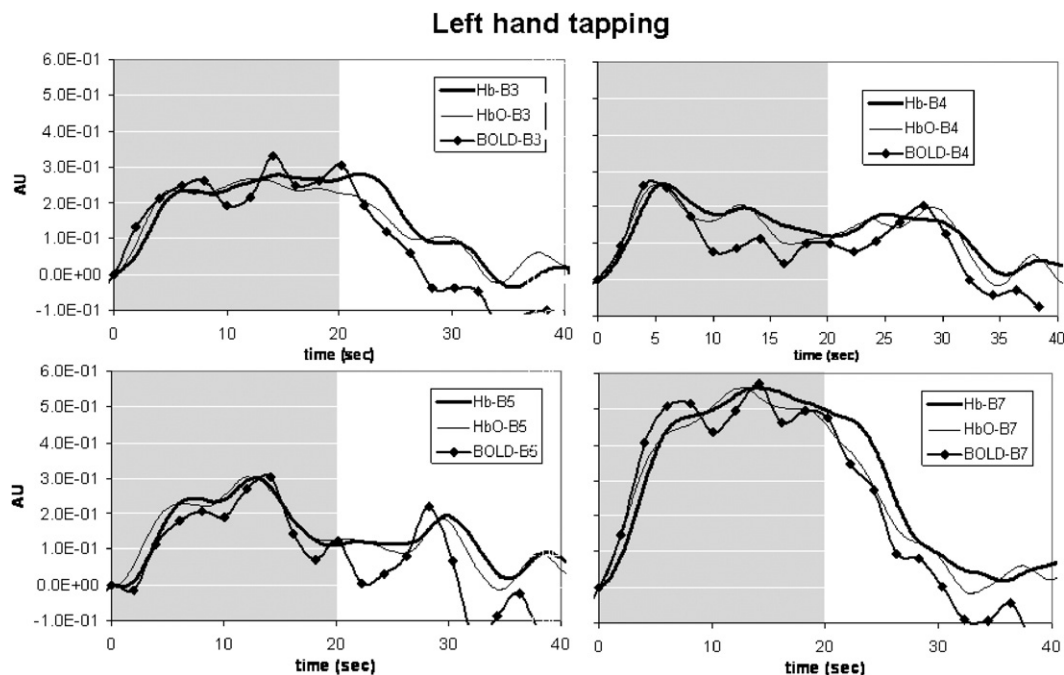


Fig. 6. Temporal traces of  $-\Delta[\text{Hb}]$ ,  $\Delta[\text{HbO}]$  and  $BOLD_{PMA}$  measured at channels B-3, B-4, B-5, B-7 (see Fig. 1 for their location on the head) during 20 s of left hand tapping (shaded area) and 20 s of rest. The temporal profiles have been normalized (and the  $\Delta[\text{Hb}]$  trace inverted) for comparison.

notice that the values of the correlation coefficients are highly significant: if we apply a  $t$ -test for the correlation coefficient in order to investigate if the difference between the sample values of  $r$  and zero is statistically significant, even for the case of  $r=0.63$  we obtain a value of  $p<0.005$ . We point out that if we check all of the possible cross correlations between all channels, we do sometimes find values of the correlation coefficients that are comparable or even higher than those obtained for the correlations within the same channel. In all of these cases, the temporal profiles at different channels have similar features, as opposed to those shown in Fig. 6. These results, despite the crude approximations used in determining the spatial weight function, make our point that a proper weight function for the raw BOLD data should be used for a meaningful and quantitative comparison with NIRS data.

In Fig. 7, we compare the temporal traces of  $-\Delta[\text{Hb}]$ ,  $\Delta[\text{HbO}]$ , and  $BOLD_{PMA}$  measured at channels C-10, C-11, C-15, D-15 (see Fig. 1 for the location of these optical channels) during right hand tapping. The calculation of  $BOLD_{PMA}$  was performed using  $k=0.20 \text{ mm}^{-1}$  (which corresponds, for example, to an absorption coefficient of  $0.011 \text{ mm}^{-1}$  and a reduced scattering coefficient of  $1.2 \text{ mm}^{-1}$ ). This choice of  $k$ , although slightly different from the previous one used for the left hand tapping, does not cause any significant change in the temporal trend of the  $BOLD_{PMA}$  as it will be shown later. For the comparison of the temporal trends, we have introduced an arbitrary normalization factor, and the trend of  $\Delta[\text{Hb}]$  has been inverted. At channel C-10,  $BOLD_{PMA}$  correlates better with  $-\Delta[\text{Hb}]$  than with  $\Delta[\text{HbO}]$ . At the other channels shown in Fig. 7,  $\Delta[\text{HbO}]$  and  $-\Delta[\text{Hb}]$  show similar temporal trends, whereas the  $BOLD_{PMA}$  trace visibly lags behind  $\Delta[\text{HbO}]$  and  $-\Delta[\text{Hb}]$  immediately after the onset of hand tapping. A quantitative analysis of the correlation between NIRS and  $BOLD_{PMA}$  data in the time interval 2–30 s typically yields lower values for the correlation coefficient than for the left hand tapping

case of Fig. 6. For example:  $r_{-\Delta[\text{Hb}]-BOLD}=0.72, 0.87, 0.62, 0.44$ , and  $r_{\Delta[\text{HbO}]-BOLD}=-0.51, 0.78, 0.68, 0.54$  at channels C-10, C-11, C-15, and D-15, respectively. At the same time, the correlation coefficients across different channels often yields comparable or higher values than those calculated within the same channel. For example, the data of  $-\Delta[\text{Hb}]$  at channel C-11 yields a correlation coefficient of 0.88 with the  $BOLD_{PMA}$  data at channel C-15, and 0.91 with the  $BOLD_{PMA}$  data at channel D-15. Similar examples of high correlation coefficient values across channels can be found for  $\Delta[\text{HbO}]$  and  $BOLD_{PMA}$ . We can summarize these results by observing that left hand tapping (Fig. 6) has shown a cortical response to activation with a stronger spatial dependence than for the case of right hand tapping (Fig. 7). The increase in cerebral  $[\text{HbO}]$  and decrease in cerebral  $[\text{Hb}]$  during finger tapping has been reported by several groups and it is a well-established response to brain activation. This behavior is assigned to an increased blood flow, which overcompensates the increased cerebral metabolic rate of oxygen ( $\text{CMRO}_2$ ) associated with neuronal activation. Since the work of Fox et al. (1998), the puzzle of the unbalance between oxygen supply and  $\text{CMRO}_2$  in the activated area has not yet been unraveled.

The  $\Delta[\text{Hb}]$ ,  $\Delta[\text{HbO}]$  and  $BOLD_{PMA}$  data for all source-detector channels can be backprojected to generate spatial maps at any given time (Franceschini et al., 2000). Fig. 8 shows the maps of  $\Delta[\text{Hb}]$ ,  $-\Delta[\text{HbO}]$  and  $-BOLD_{PMA}$  recorded on the contralateral side of the tapping hand at 6 s after the onset of (a) left or (b) right hand tapping. The  $BOLD_{PMA}$  maps were calculated using  $k=0.20 \text{ mm}^{-1}$ . There is a striking similarity between the NIRS maps and the corresponding  $BOLD_{PMA}$  maps. While the fine details of the images are not meaningful (we recall that each image is obtained by backprojecting just ten independent data points), there is a visible congruence between the signals recorded with NIRS and fMRI at the various NIRS channel locations.

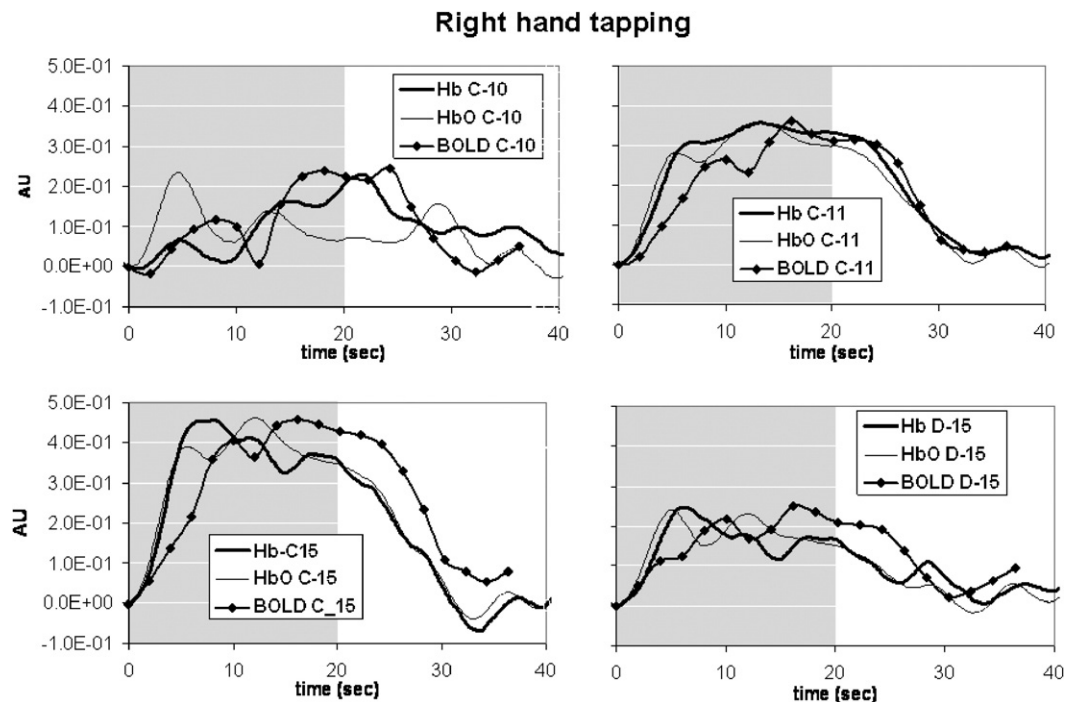


Fig. 7. Temporal traces of  $-\Delta[\text{Hb}]$ ,  $\Delta[\text{HbO}]$  and  $BOLD_{PMA}$  measured at channels C-10, C-11, C-15, D-15 (see Fig. 1 for their location on the head) during 20 s of right hand tapping (shaded area) and 20 s of rest. The temporal profiles have been normalized (and the  $\Delta[\text{Hb}]$  trace inverted) for comparison.

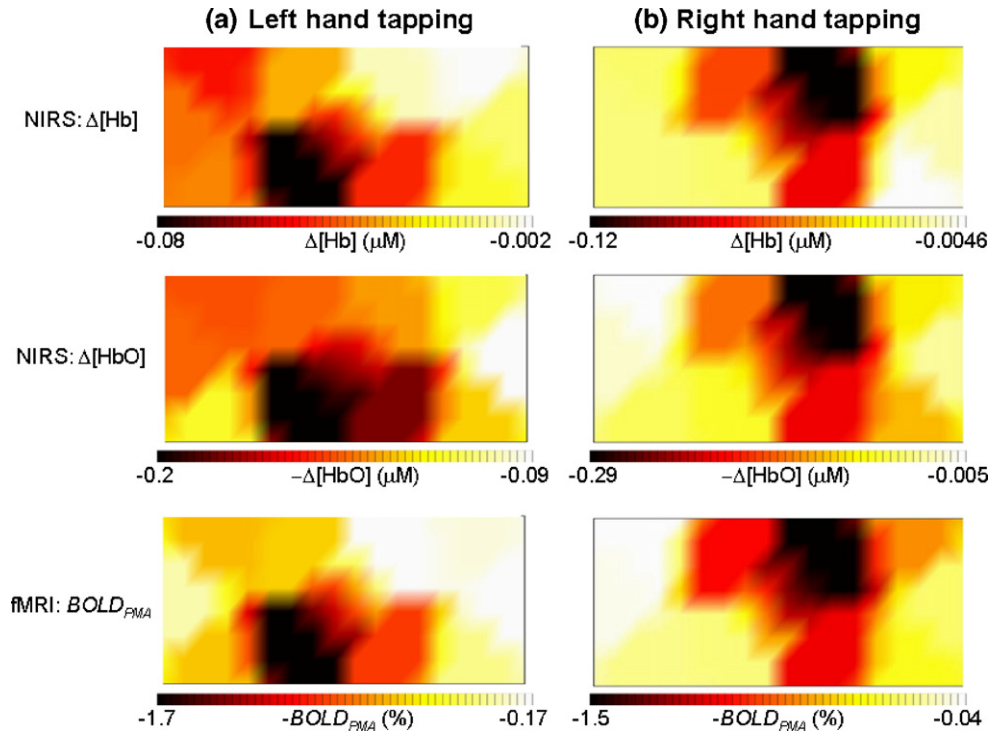


Fig. 8. Spatial maps of  $\Delta[\text{Hb}]$  (top panels),  $-\Delta[\text{HbO}]$  (middle panels), and  $-BOLD_{PMA}$  (bottom panels) measured 6 s after the onset of hand tapping on the brain side contralateral to the tapping hand. (a) left hand tapping (left panels); (b): right hand tapping (right panels).

To study the relationship between data at different source-detector channels, i.e., at different positions, we have considered the ratio between the values of a given quantity ( $\Delta[\text{Hb}]$ ,  $\Delta[\text{HbO}]$ ,

or  $BOLD_{PMA}$ ) measured at two different positions. Fig. 9 shows the temporal trends of such ratios for the channels showing the largest activation; namely B-7/A-7, A-7/B-3, for left hand tapping (panel

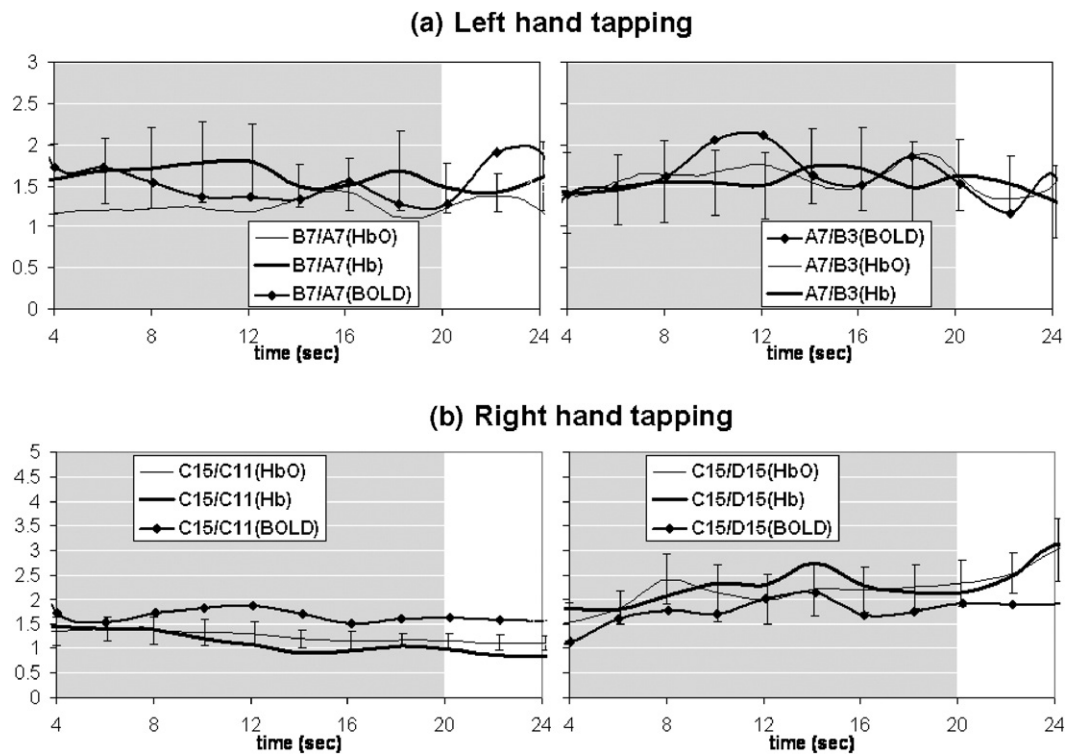


Fig. 9. Ratio of the amplitudes of NIRS data ( $\Delta[\text{Hb}]$  and  $\Delta[\text{HbO}]$ ), and  $BOLD_{PMA}$  data measured at two NIRS channel locations (as indicated in each panel) in the time range 4–24 s. (a) Left hand tapping; (b) right hand tapping. The tapping periods are indicated by the shaded area. The error is plotted for the  $\Delta\text{Hb}$  ratios and for  $\Delta\text{HbO}$  ratios in panels (a) and (b), respectively.

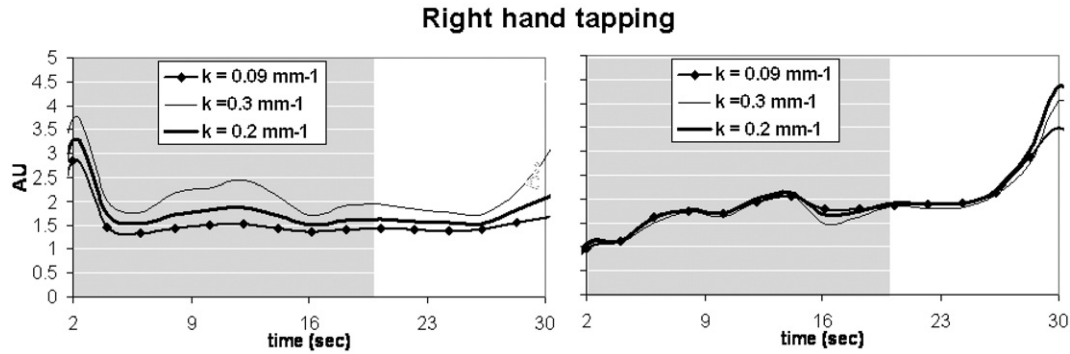


Fig. 10. Ratio of the amplitudes of  $BOLD_{PMA}$  data measured at two NIRS channel locations (C-15/D-11 and C-15/D-15, left and right panel, respectively) in the time range 2–30 s during right hand tapping. The three traces of the  $BOLD_{PMA}$  ratio correspond to three different values of  $k$ : 0.09, 0.20, and 0.30  $\text{mm}^{-1}$ .

(a)), and C-15/C-11, C-15/D-15 for right hand tapping (panel (b)). The ratios were calculated in the time range 4–24 s in order to avoid the low signals associated with the early and late times in the tapping/rest period. From Fig. 9, one can see that there is a good quantitative agreement between the spatial dependence of the NIRS and fMRI data, which generally falls within the experimental errors. This comparison of the spatial features of the NIRS and fMRI data requires a spatial weight function, such as the one that we have used here (Eq. (1)), for the calculation of a spatially confined BOLD signal.

As shown by Fig. 5, the value of the effective attenuation coefficient  $k$  affects the size and distribution of the photon-hitting density (Eq. (1)) that is used as the weight function in the spatial weighted average of the standard BOLD signal. As a result, the newly proposed  $BOLD_{PMA}$  depends on the value of  $k$ . Fig. 10 shows the  $BOLD_{PMA}$  ratios between channels C-15/C-11 and C-15/D-15 for the right hand tapping case and for three values of  $k$  (0.09, 0.20, and 0.30  $\text{mm}^{-1}$ ) that cover a wide range of optical coefficients. The ratio C-15/D-15 is not significantly affected by the value of  $k$ , while the ratio C-15/C-11 shows to be more sensitive to  $k$ , but still within the range of experimental errors.

## Conclusion

In this concurrent fMRI-NIRS study, the new proposed method for calculating the BOLD signal has shown a clear potential for carrying out a quantitative comparison of BOLD and NIRS data. We have shown that a weighted average of the raw BOLD signal should be considered for appropriate comparison with NIRS data. In particular, we have found (Figs. 6 and 7) that the photon-migration-averaged BOLD signal ( $BOLD_{PMA}$ ) typically correlates better with the changes of oxy- and deoxy-hemoglobin measured at the corresponding NIRS channel location. We argue that the newly defined BOLD signal should be used in the analysis of concurrent fMRI-NIRS studies. For example, whenever the evolution of the two species of hemoglobin is out of phase (phase shift different from  $\pi$ ), we suggest that the newly proposed BOLD signal should be used to investigate the level of correlation between BOLD and either  $\Delta[\text{Hb}]$  or  $\Delta[\text{HbO}]$ . The discrepancies of such correlation studies in the literature have been assigned to the method of optical data acquisition (Toronov et al., 2003) or to the hemodynamic and vascular compartment at the origin of BOLD and NIRS signals (Yamamoto and Kato, 2002). Here, we suggest another possible

reason in the fact that the standard BOLD signal does not take into account the spatial region of sensitivity for NIRS data, and for this reason we have introduced a photon-hitting density weighted BOLD signal ( $BOLD_{PMA}$ ). The exact form of this photon-hitting density function can be rather complex and dependent on the three-dimensional distribution of the tissue optical properties and on the geometry of the subject's head. We have proposed to use a semi-infinite homogeneous model for the calculation of this function, arguing that the average optical properties of the sampled area and the location of the illumination-collection points with respect to the region of BOLD activation play the major role in determining the  $BOLD_{PMA}$  signal. More accurate analytical functions, for example from a layered model, can be applied at the expense of an increased computation time.

In the case study presented here, the spatial and temporal correlations between  $BOLD_{PMA}$  signals and NIRS data are excellent. In particular, Fig. 6 shows a striking agreement between the channel-to-channel variability in the  $BOLD_{PMA}$  and NIRS signals. We believe that the proposed method for the calculation of BOLD signal is important for a meaningful and quantitative comparison of fMRI and NIRS data. However, we should remind that the newly defined way of BOLD calculation takes into account only of the spatial dependence of the BOLD signal within the region of activation for comparison with NIRS. Therefore, this method does not guarantee that the  $BOLD_{PMA}$  provides always a match with NIRS signal, since: (1) the origin of the BOLD signal is not exactly the same as in NIRS (as discussed in the Introduction); (2) given a certain region of brain activation different vascular compartment can be selected by fMRI by changing the static field strength. On the contrary this is not possible with NIRS, which is mainly sensitive to the capillary and small veins compartments. The possibility to select the vascular compartment in fMRI is an additional parameter that we should always bear in mind when comparing BOLD and NIRS data. The excellent comparison shown in Fig. 6 might be due to the particular field strength used for the fMRI data (3T) which makes the BOLD signal sensitive to both large veins and capillary compartments.

## Acknowledgments

We thank Dr. Bruce Ehrenberg for the useful discussions. This work was supported by the National Institutes of Health, Grants No. DA14178, K25DA14013, and by the National Science Foundation, Award No. BES-93840.

## References

- Boas, A.D., Gaudette, T., Strangman, G., Cheng, X., Marota, J.J.A., Mandeville, J.B., 2001. The accuracy of Near Infrared spectroscopy and imaging during focal changes in cerebral hemodynamics. *NeuroImage* 13, 76–90.
- Boxerman, J.L., Bandettini, P.A., Kwong, K.K., Baker, J.R., Davis, T.L., Rosen, B.R., Weisskoff, R.M., 1995. The intravascular contribution to fMRI signal change: Monte Carlo modeling and diffusion-weighted studies in vivo. *Magn. Reson. Med.* 34, 4–10.
- Buxton, R.B., Frank, L.R., 1997. A model for the coupling between cerebral blood flow and oxygen metabolism during neural stimulation. *J. Cereb. Blood Flow Metab.* 17, 64–72.
- Buxton, R.B., Wong, E.C., Frank, L.R., 1998. Dynamics of blood flow and oxygenation changes during brain activation: the balloon model. *Magn. Reson. Med.* 39, 855–864.
- Buxton, R.B., Uludag, K., Dubowitz, D.J., Liu, T.T., 2004. Modeling the hemodynamic response to brain activation. *NeuroImage* 23, S220–S223.
- Chance, B., Anday, E., Nioka, S., Zhou, S., Hong, L., Worden, K., Li, C., Murray, T., Ovetzky, Y., Pidikiti, D., Thomas, R., 1998. A novel method for fast imaging of brain function, non-invasively, with light. *Opt. Express* 2, 411–423.
- Csibra, G., Henty, J., Volein, A., Elwell, C., Tucker, L., Meek, J., Johnson, M.H., 2004. Near infrared spectroscopy reveals neural activation during face perception in infants and adults. *J. Pediatr. Neurol.* 2, 85–89.
- Del Bianco, S., Martelli, F., Zaccanti, G., 2002. Penetration depth of light re-emitted by a diffusive medium: theoretical and experimental investigation. *Phys. Med. Biol.* 47, 4131–4144.
- Fantini, S., 2002. A hemodynamic model for the physiological interpretation of in vivo measurements of the concentration and oxygen saturation of hemoglobin. *Phys. Med. Biol.* 47, N248–N257.
- Fantini, S., Franceschini, M.A., 2002. Frequency-domain techniques for tissue spectroscopy and imaging. In: Tuchin, V. (Ed.), *Optical Biomedical diagnostic*. SPIE Press, Bellingham, pp. 405–453.
- Fantini, S., Hueber, D., Franceschini, M.A., Gratton, E., Rosenfeld, W., Stubblefield, P.G., Maulik, D., Stankovic, M.R., 1999. Non invasive optical monitoring of the newborn piglet brain using continuous-wave and frequency-domain spectroscopy. *Phys. Med. Biol.* 44, 1543–1563.
- Feng, S., Zeng, F., Chance, B., 1995. Photon migration in the presence of a single defect: a perturbation analysis. *Appl. Opt.* 34, 3826–3837.
- Fox, P.T., Raichle, M.E., Mintum, M.A., Dence, C., 1998. Nonoxidative glucose consumption during focal physiologic neural activity. *Science* 241, 451–460.
- Franceschini, M.A., Toronov, V., Filiaci, M.E., Gratton, E., Fantini, S., 2000. On-line optical imaging of the human brain with 160-ms temporal resolution. *Opt. Express* 6, 49–57.
- Hoshi, Y., Tamura, M., 1993. Detection of dynamic changes in cerebral oxygenation coupled to neuronal function during mental work in man. *Neurosci. Lett.* 150, 5–8.
- Kennan, R.P., Horovitz, S.G., Maki, A., Yamashita, Y., Koizumi, H., Gore, J.C., 2002. Simultaneous recording of event-related auditory oddball response using transcranial near infrared optical topography and surface EEG. *NeuroImage* 16, 587–592.
- Kim, S.-G., Rostrup, E., Larsson, H.B.W., Ogawa, S., Paulson, O.B., 1999. Determination of relative CMRO<sub>2</sub> from CBF and BOLD changes: Significant increase of oxygen consumption rate during visual stimulation. *Magn. Reson. Med.* 41, 1152–1161.
- Matcher, S.J., Cope, M., Delpy, D.T., 1993. Use of the water absorption spectrum to quantify tissue chromophore concentration changes in near-infrared spectroscopy. *Phys. Med. Biol.* 38, 177–196.
- Obata, T., Liu, T.T., Miller, K.L., Luh, W., Wong, E.C., Frank, L.R., Buxton, R.B., 2003. Discrepancies between BOLD and flow dynamics in primary and supplementary motor areas: application of the balloon model to the interpretation of BOLD transients. *NeuroImage* 21, 144–153.
- Ogawa, S., Menon, R.S., Tank, D.W., Kim, S.G., Merkle, H., Ellermann, J.M., Ugurbil, K., 1993. Functional brain mapping by blood oxygenation level-dependent contrast magnetic resonance imaging. A comparison of signal characteristics with a biophysical model. *Biophys. J.* 64, 803–812.
- Sassaroli, A., Fantini, S., 2004. Comment on the modified Beer-Lambert law for scattering media. *Phys. Med. Biol.* 49, N255–N257.
- Schotland, J.C., Haselgrove, J.C., Leigh, J.S., 1993. Photon hitting density. *Appl. Opt.* 32, 448–453.
- Seiyama, A., Seki, J., Tanabe, H.C., Sase, I., Takatsuki, A., Miyauchi, S., Eda, H., Hayashi, S., Imaruoka, T., Iwakura, T., Yanagida, T., 2004. Circulatory basis of fMRI signals: relationship between changes in the hemodynamic parameters and BOLD signal intensity. *NeuroImage* 21, 1204–1214.
- Siegel, A.M., Culver, J.P., Mandeville, J.B., Boas, D.A., 2003. Temporal comparison of functional brain imaging with diffuse optical tomography and fMRI during rat forepaw stimulation. *Phys. Med. Biol.* 48, 1391–1403.
- Strangman, G., Culver, J.P., Thompson, J.H., Boas, D.A., 2002. A quantitative comparison of simultaneous BOLD fMRI and NIRS recordings during functional brain activation. *NeuroImage* 17, 719–731.
- Strangman, G., Franceschini, M.A., Boas, A.D., 2003. Factors affecting the accuracy of near-infrared spectroscopy concentration calculations for focal changes in oxygenation parameters. *NeuroImage* 18, 865–879.
- Toronov, V., Franceschini, M.A., Filiaci, M.E., Fantini, S., Wolf, M., Michalos, A., Gratton, E., 2000. Near-infrared study of fluctuations in cerebral hemodynamics during rest and motor stimulation: temporal analysis and spatial mapping. *Med. Phys.* 27, 801–815.
- Toronov, V., Webb, A., Choi, J.H., Wolf, M., Safonova, L., Wolf, U., Gratton, E., 2001. Study of local cerebral hemodynamics by frequency-domain near-infrared spectroscopy and correlation with simultaneously acquired functional magnetic resonance imaging. *Opt. Express* 9, 417–427.
- Toronov, V., Walker, S., Gupta, R., Choi, J.H., Gratton, E., Hueber, D., Webb, A., 2003. The roles of changes in deoxyhemoglobin concentration and regional cerebral blood volume in the fMRI BOLD signal. *NeuroImage* 19, 1521–1531.
- Uludag, K., Steinbrink, J., Villringer, A., Obrig, H., 2004. Separability and cross talk: optimizing dual wavelength combinations for near-infrared spectroscopy of the adult head. *NeuroImage* 22, 583–589.
- Watanabe, E., Maki, A., Kawaguchi, F., Yamashita, Y., Koizumi, H., Mayanagi, Y., 1998. Non-invasive assessment of language dominance with near-infrared spectroscopic mapping. *Neurosci. Lett.* 256, 49–52.
- Wolf, M., Wolf, U., Toronov, V., Michalos, A., Paunescu, L.A., Choi, J.H., Gratton, E., 2002. Different time evolution of oxyhemoglobin and deoxyhemoglobin concentration changes in the visual and motor cortices during functional stimulation: a near-infrared spectroscopy study. *NeuroImage* 16, 704–711.
- Yamamoto, T., Kato, T., 2002. Paradoxical correlation between signal in functional magnetic resonance imaging and deoxygenated hemoglobin content: a new theoretical explanation. *Phys. Med. Biol.* 47, 1121–1141.
- Yamashita, Y., Maki, A., Koizumi, H., 2001. Wavelength dependence of the precision of noninvasive optical measurements of oxy-, deoxy-, and total-hemoglobin concentration. *Med. Phys.* 28, 1108–1114.